XX Computational Photochemistry: advances in 2022 – 2023

M. Navarrete-Miguel[a], J. Cuéllar-Zuquin[a], J. Carmona-García[a], A. M. A. Abdelgawwad[a], I. Soriano-Díaz[a], J. C. Roldao[a], D. Halder[a], A. Borrego-Sánchez[b], A. Francés-Monerris[a], A. Giussani[a], J. Segarra-Martí[a], and D. Roca-Sanjuán[a*].

[a] Instituto de Ciencia Molecular, Universitat de València, P.O.Box 22085, ES-46071 València, Spain, [b] Departamento de Farmacia y Tecnología Farmacéutica y Parasitología, Universitat de València, P.O.Box 22085, ES-46071 València, Spain

*corresponding email address: daniel.roca@uv.es

ABSTRACT/WEB SUMMARY

Computational Photochemistry allows to obtain a description of light-induced chemical phenomena reaching the molecular size-scale and femtosecond time-scale resolutions. In the period 2022-2023, we can find a significant increase on the use of tools of computational photochemistry in materials science, as compared to previous years, maintaining the relative amount of works on the areas of biology, medicine, nanotechnology and atmospheric chemistry. To illustrate such advances in this field, we have chosen here representative applied studies focused on the non-radiative decay paths of DNA nucleobases, the photoreductive repair or thymine dimers, photosensitizers generating singlet oxygen and

oxygen-independent photoactivated therapies, conjugated organic oligomers of interest in optoelectronic devices, ionic transition metal complexes for light emitting electrochemical cells, and sulphur chemistry in planetary atmospheres. In this occasion, we also describe the new features implemented in one of the quantum-chemistry packages of software specialized in photochemistry, the OpenMolcas program.

1 Introduction and statistics of articles published in 2022-2023

Computational Photochemistry is the field of research in which the tools of quantum chemistry are used to study the chemical transformation induced in molecular systems irradiated by light with wavelengths short enough to populate excited electronic states. It belongs to the more general area of quantum chemistry of the excited electronic states (QCEX), which also includes other phenomena such as excited state chemistry induced not by light absorption but by a thermal reaction (dark photochemistry) and luminescence (fluorescence and/or phosphorescence) induced by a thermal reaction (chemiluminescence).

As we have done in our previous contributions, to see the progress on the field and the trends in the period 2022-2023, we have searched for the most common topics in articles focused on multiconfigurational quantum chemistry (MQC) and on the excited electronic state chemistry published in those years. To know these trends, we conducted searches using specific keywords: (CASPT2 or multiconfig*) and (photored* or photox* or photochem* or photodis* or photocat* or photodim* or photolys* or photosens* or photoles* or chemilumin* or "nonradiative"). We have restricted the search to multiconfigurational quantum chemistry to capture those studies that provide a deeper analysis on the electronic-structure details of excited-state chemistry. Nevertheless, throughout this book chapter we shall also include examples of works using other methodologies, like time-dependent density functional theory (TD-DFT), which if properly benchmarked are able to provide relative trends. The resulting insights of the search of articles on computational photochemistry with the mentioned keywords are depicted in *Figure 1*.

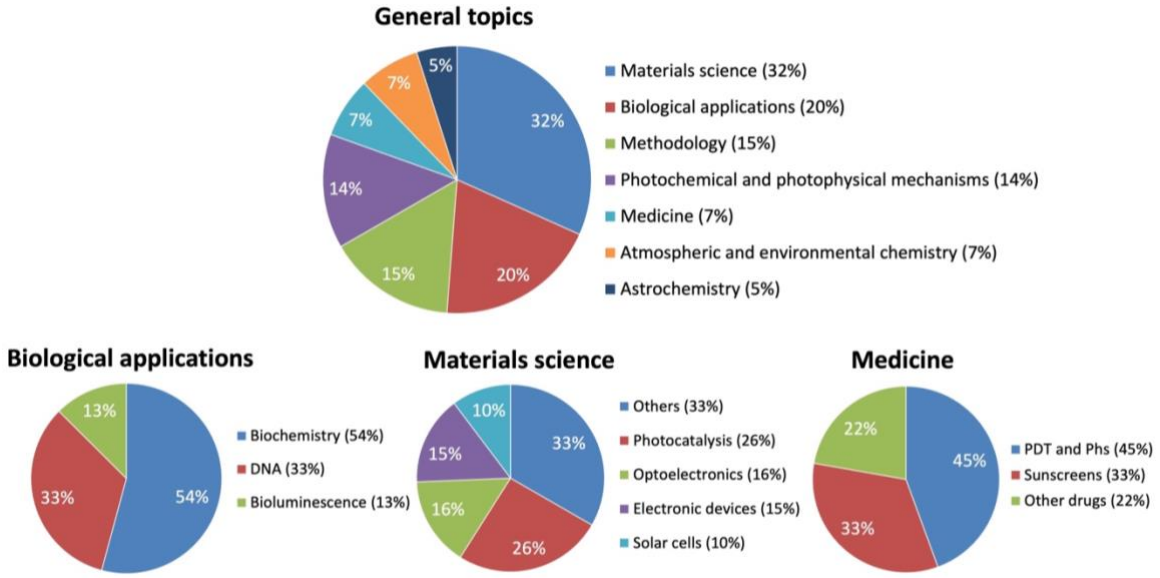

Figure 1 Statistics based on MQC studies published during 2022 and 2023. Various general topics are identified (a). Some of these can be further divided into subsections: studies with applications in biology area (b), articles related to materials science (c), and investigations with medical applications (d). These statistics are derived from 123 articles indexed in the ISI Web of Science.[1]

Upon analysing the articles published in 2022 and 2023, it can be observed that the majority focus on materials science, constituting 32% of the total. Within materials science, topics such as photocatalysis (26%), optoelectronics (16%), electronic devices (15%), solar cells (10%), and various other applications (33%), are found. In the last category, we observe, for instance, the design and synthesis of novel molecular materials, studies of photo-properties, etc. Additionally, biological applications emerge as the second most prevalent theme, encompassing areas like biochemistry (54%), DNA studies (33%), and bioluminescence (13%) in a lesser extent. Methodology developments and benchmarking ranks third, accounting for 15% of the publications, with works centred around methodological implementation or enhancement, alongside machine learning applications. A notable portion of the research explores into photophysical and photochemical mechanisms (14%). Medical themes also get attention (7%), including photodynamic therapy and photosensitiser studies (45%), sunscreens (33%), and other drugs (22%). Moreover, studies concerning atmospheric

and environmental chemistry (7%) and, to a lesser extent, molecules pertinent to astrochemistry (5%) have been also conducted.

Comparing these statistics with those from works published in 2020 and 2021, it is observed that studies and investigations related to biological applications have remained steady at approximately 20% of the total papers analysed. In contrast, research in materials science using MQC has notably increased in importance over the past few years, now occupying the top spot in published articles. This year, like in the 2018-2019 period, we again see articles related to electronic devices and solar cells, although their relevance is low. As in previous statistics, medicine, atmospheric chemistry, and astrochemistry remain the less frequently addressed topics.

In the following sections, we shall begin by describing some new implementation in one of the most popular programs specialized in photochemistry, OpenMolcas. Next, we will include examples of studies representative of the advances of computational photochemistry in the period 2022-2023, divided in the following categories: photobiology, photobiomedicine, photonanotechnology and atmospheric photochemistry.

2 Software in Photochemistry

In (computational) photochemistry, one of the main challenges is to correctly describe molecular systems in terms of both wavefunction (with either a single- or many-determinantal solutions) and energy (including static and dynamic electron correlation contributions) for the different electronic states involved in a given photo-reaction. Potential energy surfaces of ground and electronic excited states present many instances of energy degeneracies or “crossing points”, known as conical intersections or singlet-triplet crossings, which were once believed to be rare occurrences but that have been shown over the last couple decades to be prominent in most photochemical processes. These crossings are intrinsically difficult to simulate, but new theoretical developments have been steadily introduced enabling their routine modelling.

Nowadays there are several programs like OpenMolcas,[2] ORCA,[3] Bagel,[4] amongst others, which enclose different approaches and methodologies for modelling excited-state driven processes, including the accurate simulation of elusive conical intersections. In 2023 the latest developments in OpenMolcas were published:[2] this appends several recent implementations that extend and/or improve functionality. Amongst them, we are going to review some of those that extend our capabilities in the study of photochemical processes.

As mentioned above, a correct description of the different partaking electronic states is crucial to simulate photo-reactions. In this context, an efficient and accurate method to obtain both wavefunctions and energies is necessary, and popular method is the multiconfigurational second-order perturbation theory (PT2) class of methods available in OpenMolcas, particularly applied on top of a complete active space (CAS) reference (i.e. CASPT2). These include now analytic first-order derivatives for most versions of CASPT2, including nonadiabatic coupling vectors, which may be used in geometry optimisation calculations such as minimum energy conical intersections or for on-the-fly evaluations in non-adiabatic molecular dynamics, both aspects of importance in photochemistry.

New variants of CASPT2 are now available, including the extended dynamically weighted CASPT2 (XDW-CASPT2)[5] and rotated multistate CASPT2 (RMS-CASPT2).[6] These variants aim to maintain the accuracy of multistate (MS-)CASPT2[7] for relative energies while ensuring smooth potential energy surfaces throughout the conformational space as obtained in the extended multistate (XMS-CASPT2) formulation.[8] Key improvements include rotating CASSCF wave functions to diagonalise the state-averaged Fock operator and partitioning the Hamiltonian for each model state separately using state-specific Fock operators constructed with a dynamic weighting scheme and the rotated CASSCF wave functions.

Cost-wise, these methodologies rely on many-body perturbation theory (MBPT; normally up to 2nd order) and are strongly limited by molecular and/or basis set size. A way around this is provided by the Frozen Natural Orbital (FNO) approach implemented in OpenMolcas for CASSCF,[9,10] which has recently been extended to restricted active space (RAS) approaches

leading to the FNO-RASPT2 method, thereby increasing its functionality. In this new approach,[2] a level shift (denoted by σ) via regularization is performed on top of the approximated (virtual-virtual block) density matrix used for the orbital selection stage prior to truncating: this allows removing degeneracies in occupation numbers and enables a more clear-cut distinction of those orbitals that are to be deleted from the perturbation step. In this way, costs are considerably reduced by removing the less relevant secondary orbitals. This regularization technique has also been implemented within the context of the intruder state problem,[11] as it helps removing problematic denominators in the second-order perturbation energy, similarly to how it is done within the well-known imaginary level shift.[12]

In *Figure 2*, an example of FNO-RASPT2 study is provided applied to N-((1E,2E,4E,6E)-nona-2,4,6,8-tetraen-1-ylidene)methanaminium (methanaminium). This molecule was selected due to its similarities with the biologically relevant Protonated Schiff Base 11 (PSB-11), which is the chromophore of Rhodopsin, the protein which mediates the first events in vision. For the purposes of testing the FNO-RASPT2 implementation, all valence π/π* orbitals included in the active space (leading to 10 electrons in 10 orbitals) were divided between RAS1 and RAS3 subspaces according to whether they were occupied (RAS1) or unoccupied (RAS3), leading to (10,2,2;5,0,5).[13]

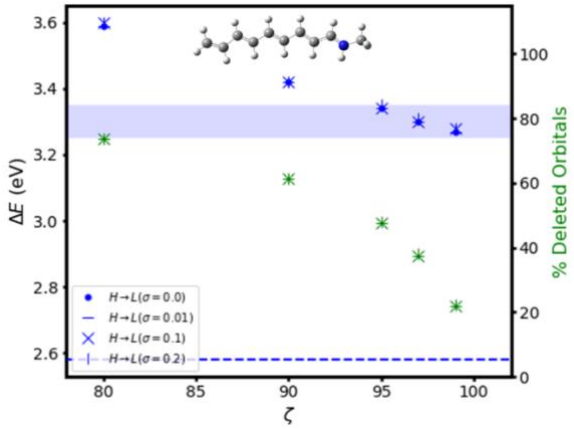

Figure 2 FNO-RASPT2 simulation the methanaminium molecule: 4 different level shifts (σ) were used ranging from 0.0 to 0.2 in the energy calculation. The blue shaded area represents

the threshold of 0.1 eV that was applied to the original transition energy (CD-RASPT2) and that was used as the reference, while the dashed line represents the CD-CASPT2 result.

Figure 2 shows how by retaining 95% of the dynamic electron correlation in the calculation, which leads to the removal of ~60% of the secondary orbitals, results comparable to those obtained with Cholesky decomposition-based RASPT2 (CD-RASPT2) (i.e. the full calculation with 100% secondary orbitals included) are achieved. This paves the way for computing larger and more realistic molecular systems, and thus extends the applicability of CASPT2/RASPT2 methodologies.

OpenMolcas also offers an alternative technique to include electron correlation on top of a CASSCF wave function, namely Multiconfiguration Pair-Density Functional Theory (MC-PDFT). This method combines the appealing favourable scaling of density functional theory (DFT) with multiconfiguration wavefunction theory to treat inherently multiconfigurational systems with near-degeneracy correlation effects,[14,15] such as those often present in photochemistry. The implementation has been extended to include new types of on-top functionals,[16–18] as well as the evaluation of analytic gradients.[19–22] The latter have been interfaced with nonadiabatic molecular dynamics software SHARC,[23,24] enabling ab initio non-adiabatic molecular dynamics simulations at affordable computational cost.

An important aspect of OpenMolcas that considerably increases its functionalities is the ease with which it may be interfaced with external programs. Some of these programs are: COBRAMM,[25] a program package used for the simulation of transient electronic spectroscopy from first principles; SHARC,[23,24] a package for running non-adiabatic dynamics simulations; or MULTISPEC,[26] a program for the calculation of gas-phase electronic spectra based on the nuclear ensemble approach (NEA).[27] An interesting feature recently included within MULTISPEC is the use of Gaussian Mixture Models (GMM), an unsupervised machine learning (ML) algorithm which avoids the phenomenological broadening underlying the NEA formalism.[28] *Figure 3* shows an example in which this program was used, and a comparison of the different methods implemented in it. The applicability of the program was tested, and it

was extended beyond what was initially proposed by simulating photoelectron spectra not considered in the original work.[28,29]

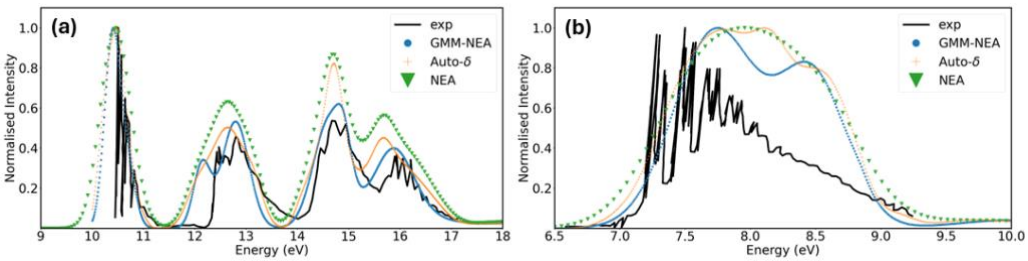

Figure 3 a) Photoelectron and b) absorption spectrum of ethylene obtained with different methods implemented in MULTISPEC program compared with the experimental data registered in the gas phase. Reprinted from ref [29], Copyright (2024), with permission from Elsevier.

3 Computational Photobiology

3.1 DNA photostability

Nucleobases are the chromophoric (i.e. light-absorbing) building blocks of our genetic material, known as DNA (deoxyribonucleic acid). These molecules are particularly resilient against radiation exposure effectively making them photostable: this is believed to have been crucial in the natural selection of these molecules to encode our genetic material during prebiotic times, when ultraviolet (UV)-exposure was prominent, hence ensuring correct replication and the perpetuation of life.[30–32] Photostability in this context therefore refers to the ability to dissipate excess energy after absorption on ultrafast time scales and is rationalised through the accessibility of conical intersections (CIs) connecting the potential energy surfaces (PESs) of the excited and ground states, thus enabling an efficient radiation-less deactivation process.

Much of this photostability therefore hinges on CI-mediated reactivity, as these key structures act as population funnels between excited and (excited and) ground electronic states. CIs are structures that are intrinsically difficult to model: they embody adiabatic state energy degenerations, which often require multiconfigurational methods for their appropriate

description as well as an even-footing consideration of electron correlation between the partaking states, and their topology and/or shape is believed to influence ensuing excited-state reactivity.[33] Moreover, CIs are yet to be directly measured experimentally (even if they have been indirectly observed)[34], which makes their theoretical characterization even more important.[35,36] A key aspect when studying reactions involving this type of critical points is the amount of correlation included in the calculation and, in this context, an exhaustive and systematic analysis on how topology is affected by the amount of static correlation included (by means of using different active spaces within CASSCF) in the calculations was performed last year by Cuéllar-Zuquin and co-workers.[37]

Active space size in CI topology was studied due to the indiscriminate use of different (and unjustified) active space sizes in many studies including hybrid quantum mechanics/molecular mechanics (QM/MM) schemes, where the relative accuracy of the model was unclear. The general procedure in this work consisted in starting from their full π (occupied and virtual) and nO/N (occupied) valence active space and reducing it according to their state-averaged natural orbital occupation numbers, eliminating in following steps those that contributed less to the calculation. With this procedure, over 300 CIs were optimised and analysed in terms of parameters $\mathcal{P}$ and $\mathcal{B}$: these allow classifying CIs in four different types (see *Figure 4*) and are based on similar parameters originally formulated by Ruedenberg and co-workers.[38]

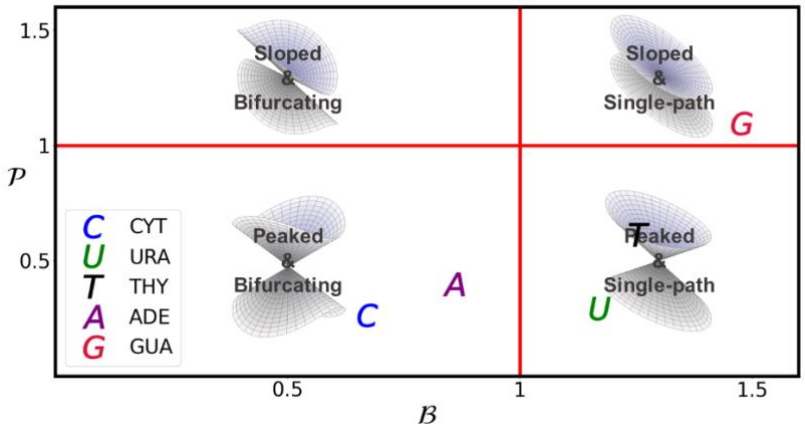

Figure 4 Summary of the classification in terms of $\mathcal{P}$ and $\mathcal{B}$, including a three-dimensional representation of the two potential energy surfaces in the branching space, for the most relevant CIs in terms of photostability for all the DNA/RNA nucleobases using the largest and therefore, the most correlated active space: $(^1\pi\pi^*/S_0)_{CI}$ and $(La(^1\pi\pi^*)/_{S0})_{CI}$.

The study considered the main conical intersections mediating ultrafast decay in DNA/RNA nucleobases, including non-adiabatic population transfer to dark states after absorption. The authors found significant discrepancies in CI topology by altering active space size, which exhibited no discernible trends. These discrepancies may originate from the inability of the current classification scheme to account for subtle changes in static electron correlation. Interestingly, changing active spaces often resulted in almost identical optimised geometries with very different topographies: this may impact significantly photochemical reactivity, as it implies the underlying potential energy surfaces (and their associated wave functions) are vastly affected by active space size.

Figure 4 also shows the topologies of $(^1\pi\pi^*/S_0)_{CI}$ and $(La(^1\pi\pi^*)/_{S0})_{CI}$, which are the CIs believed to mediate the ultrafast decay component responsible for the photostability of DNA.[39,40] Despite underpinning what are believed to be analogous decay channels,[41,42] no clear trends were found across the most correlated (i.e. with the largest and most accurate active space) calculations for the different nucleobases. Uracil and thymine (T) agree in their classification as peaked and single-path, as one would expect given their only difference is 5-methylation, but cytosine and adenine are both classified as peaked and bifurcating while guanine, despite its structural similarity to cytosine, shows a sloped and single-path topography.

Finally, *Figure 4* therefore show how CI topologies, particularly when using CASSCF potential energy surfaces, do not converge to a shared intersection type that may explain a unified ultrafast decay mechanism in DNA/RNA nucleobases. This also contrasts with previous works which point at sloped and single-path topologies as precursors of photostability due to the gradient pointing towards the recovery of the ground state.[43–45]

3.2 DNA repair

Despite the intrinsic photostability properties of nucleobases, a small quantum yield of UV irradiated DNA corresponds to photoreactivity. One of the most frequent lesions in this context is a [2+2] photocycloaddition giving rise to cyclobutane pyrimidine dimers (CPDs). Nature has also developed repair strategies for such lesions to ensure a maximum stability of the nucleic acids. Some of such repair mechanisms are based on the photo-reduction of the CPD by means of an intermediate molecule which absorbs light and reduces the pyrimidine dimer inducing in such manner the C-C bond breakings and the splitting of the two pyrimidine bases. In this field, we would like to highlight the work carried out by Rodríguez-Muñiz, et al.[46] on the ability of photorepairing T dimers by two surprising compounds, the most common lesion under oxidative stress (8-oxoguanine, OG) and the canonical guanine itself (G). The authors measured the photocleavage of the T dimer covalently linked to G and OG (hereafter, G-CPD and OG-CPD, respectively) by means of UV spectrophotometry and High-Performance Liquid Chromatography (HPLC), with yields of 2 and 7 x 10^{-3} for the canonical nucleobase and the oxidated derivative, respectively. These yields are relatively low, which is attributed to the efficiency of a back electron transfer process. Nevertheless, they are not zero and differences appear between G and OG, which are worth researching. Quantum chemistry computations based on DFT combined with experimental data allowed to determine the energetic change for the photoreductive process: $OG^*/G^* + CPD \rightarrow OG^{\bullet+}/G^{\bullet+} + CPD^{\bullet-}$, being more exergonic for OG (-0.84 eV) than for G (-0.75 eV). This difference is the major factor responsible for the higher yield of photorepair of OG. Molecular dynamics simulations were also performed to statistically analyse the relative orientations between G/OG and CPD and search for further contributions to the different quantum yield of photorepair. Differences were indeed found in the simulations. Thus, while G-CPD shows fast and frequent conformational changes, OG-CPD conformations are more stable. Three types of conformations were found for G-CPD: π-stacking between the two guanine monomers (G–G π-stacking, *Figure 5*A), π-stacking between a guanine and a T moiety of the CPD (G-T π-stacking, *Figure 5*B), and hydrogen

bonding between the guanine monomers (G–G hydrogen bonding, *Figure 5*C). For OG-CPD, two major conformations were found: π-stacking trimer between the oxoguanine molecules and the T moiety of the CPD (OG–OG–T π-stacking, *Figure 5*D) and hydrogen bonding conformation between the oxoguanines (OG–OG hydrogen bonding, *Figure 5*E). Only the G-T π-stacking conformation shall contribute positively by helping to donate the electron by π-stacking. It appears in 7% of the simulations of G-CPD and 58.2% in OG-CPD.

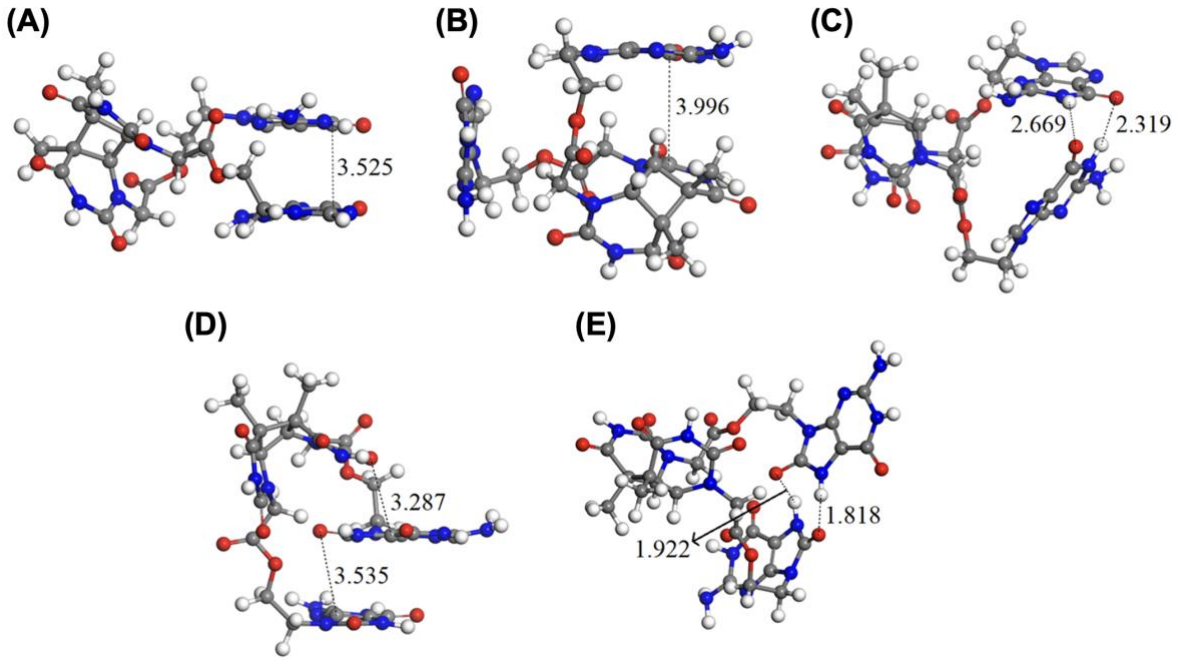

Figure 5 Stable conformations of G/OG-CPD during the MD simulations. G–G π-stacking (A), G-T π-stacking (B), G–G hydrogen bonding (C), OG–OG–T π-stacking (D), and OG–OG hydrogen bonding (E). Relevant atom distances (in Å) are highlighted. Adapted from [46] *under the Creative Commons BY 4.0 License terms.*

4 Computational Photomedicine

4.1 Phototherapies

Light-induced therapies make use of an external stimulus (light) to activate biological damage with high spatial and temporal control over the ill tissue to maximize the therapeutic effect and minimize systemic side effects[47–51] The achieved selectivity makes this approach highly

attractive to treat various health conditions, thereby stimulating cellular repair and eliminate pathogens or abnormal cells by employing specific wavelengths within the so-called therapeutic window.

4.1.1 Photodynamic therapy

One of the most successful approaches is photodynamic therapy (PDT),[47–49,52–56] which is based on the administration of light-sensitive compounds, known as photosensitizers, innocuous in the dark although able to absorb light and deliver biological damage in presence of O_2. When activated, these photosensitizers react and generate reactive oxygen species (ROS) that selectively target and destroy malignant or diseased cells. This mechanism makes PDT particularly effective in oncology, offering a minimally invasive yet highly targeted approach to cancer treatment.

A wide variety of chemical and molecular mechanisms of biological damage, which strongly depend on the chemical nature of the photosensitizer, have been developed in the last decades.[50,54,57] The years 2022 and 2023 have seen substantial advancements in both experimental and theoretical studies of PDT processes, particularly concerning novel photosensitizers. This section covers recent advances in the theoretical description of the photoprocesses that take place upon irradiation of novel organic and metal-based photosensitizers. Photosensitizers are classified based on their ability to function in the presence of oxygen, generating ROS, or under hypoxic conditions typical of solid tumors.[58,59]

Excited-state computations were used in 2023 to guide the rational design of a PDT photosensitizer based on gemcitabine (GEM),[60] a well-known chemotherapy agent. GEM is known for its short half-life in bloodstream due to a rapid deamination, necessitating high-dosing strategies for therapeutic efficacy.[60,61] The possibility to activate GEM with light and promote triplet population, a necessary step for PDT activity mediated by cellular O_2, was explored through CASSCF/MS-CASPT2/MM determinations. As a cytidine analogue, the absorption properties of GEM fall in the UVB region at 280 nm.[60] Several chemical modifications based on existing derivatives reported in the literature[61] were proposed to shift

its absorption band and enhance triplet population. The impact of the following modifications was considered: (i) O2 oxygen atom substitution with heavier S or Se, to red-shift the absorption band and enhance spin–orbit coupling, (ii) introduction of a lipophilic chain at the N7 position to improve cellular transport and block gemcitabine metabolism, and (iii) attachment of aromatic systems at the C5 position to further extend the red shift. Accurate CASSCF/MS-CASPT2/MM and time-dependent DFT (TD-DFT) results demonstrate that these chemical modifications effectively shift the absorption spectrum towards the visible range (500 nm and beyond) and significantly enhance spin–orbit coupling, crucial for efficient PDT. These results underscore the potential of developing a drug with dual applications, combining both chemotherapy and PDT.

4.1.2 Oxygen-independent photoactivated therapies

Traditional PDT photosensitizes O_2 to cause biological damage. Thus, PDT approaches require a sufficient O_2 concentration in the cellular medium to work efficiently. However, solid tumors tend to develop hypoxia conditions, resulting in a low O_2 flux that make PDT processes inefficient and thus limiting the applicability of traditional PDT.[57–59] Therefore, there is an intense search of alternative photosensitizers able to operate through oxygen-independent mechanisms or, at least, capable to deliver significant biological damage at low O2 concentration (~1%).

4.1.2.1 Nitroimidazol derivatives and DNA cross-link formation.

The experiments reported by Han et al. demonstrated that a photosensitizer based on a binitroimidazole backbone can form DNA interstrand cross-links (ICLs) after 2 hours of incubation with DNA under irradiation at 350 nm.[62] ICLs were observed through nuclear magnetic resonance, high-resolution mass spectrometry, and liquid chromatography-mass spectrometry. The timescale and the regioselectivity of the ICL formation was later characterized by our research group employing a multiscale computational protocol to study the DNA reactivity mechanism of the binitroimidazole derivative, enhancing the understanding of therapies based on photoinduced DNA damage at molecular and electronic levels.[63] In

particular, we utilized a combination of *ab initio* multiconfigurational and DFT-based quantum mechanical (QM) methods, as well as classical and hybrid QM/MM molecular dynamics (MD) simulations. Light absorption was studied by means of the CASPT2 and TD-DFT methods, identifying the absorption to a n_{NO2},p* state. Nitrogen mustard photorelease both in the S_1 state and via photoreduction, which form the reactive radical or cationic species, was studied through TD-DFT. On the S_1 surface, the cleavage of the C–N bond in nitroimidazole to release nitrogen mustard and produce a cation has an energy penalty of $\Delta E^{\ddagger}$ ~0.58 eV (13.4 kcal/mol), whereas the nitroimidazole photoreduction in the S_1 excited state by guanine is significantly exothermic (ΔE = −21.74 kcal/mol).[63]

Thermodynamics (ΔG) and kinetics ($\Delta G^{\ddagger}$) parameters for the reactions of cations and radicals with various DNA nucleobases were subsequently determined through the DFT/M06-2X functional.[63] The results showed that most cation reactions were highly exergonic with very small or absent energy barriers. MD and QM/MM MD simulations confirmed the barrierless reactivity and the picosecond timescale of the cation species reaction with specific nucleophilic positions of each DNA nucleobase in realistic biological environments. Figure 7 summarizes the mechanism of cation interaction with the most reactive positions: N3 and N7 of adenine and N7 and O6 of guanine. Once the cationic species **2** is close to the DNA hotspot, it reacts with these positions in less than 10 picoseconds, forming a link that facilitates subsequent interaction with the complementary nucleobase or the adjacent Watson–Crick base pairs upon the release of a second nitrogen mustard. This mechanism identifies GC, GT, and AT steps as the most favourable hotspots for ICL formation.[63]

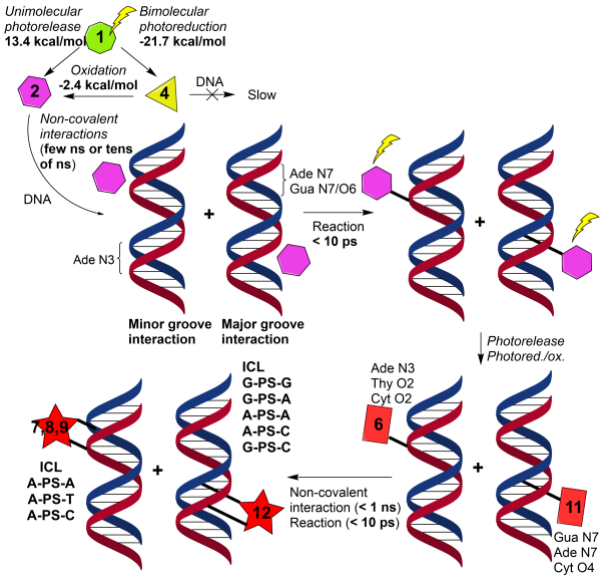

Figure 6 Schematic representation of the temporal and spatial scales for the DNA ICL mechanism between the cation and nucleobase reactive position. Reproduced with permission from reference [63] *under the Creative Commons BY 4.0 License terms.*

4.1.2.2 NO photorelease

The development of precursors and strategies to activate nitric oxide (NO) release by excitation in the so-called “therapeutic window”, with highly biocompatible and tissue-penetrating red light is of particular relevance, especially in cancer applications where the effects of this molecule can be either detrimental or beneficial depending on its doses.[50] In 2023, a combination of experimental and computational techniques studied a novel approach that combines a traditional photosensitizer, verteporfin (VTP), with a NO photodonor, named NBF-NO.[64] Biodegradable polymeric nanoparticles were designed to encapsulate a photosensitizer and a NO donor. Upon irradiation with red light, the VTP photosensitizer generates ROS and triggers the release of NO from NBF-NO, which can induce additional cytotoxic effects also in hypoxia. The polymeric nanoparticles ensure a controlled and sustained release of NO, improving the selectivity and effectiveness of the treatment. Experiments were conducted to evaluate the NO release profile and the photodynamic effects on cancer cells. The nanoparticles demonstrated efficient NO release upon red light irradiation, with a corresponding increase in ROS production. In vitro studies using cancer cell

lines revealed a significant increase in cell death compared to traditional PDT alone, highlighting the synergistic effect of combined NO release and photodynamic action.[64]

The NO photorelease upon red light irradiation of biodegradable polymeric nanoparticles was studied by using computational photochemistry tools.[64] Key properties such as absorption spectra, singlet-triplet energy gaps, and spin-orbit couplings of both VTP and NBF-NO units were used to rationalize the efficiency of intersystem crossing (ISC) and the generation of ROS observed in the experiments. The VTP→NBF-NO triplet-triplet energy transfer mechanism was established based on geometry interpolations between the lowest-lying triplet excited states localized over each molecule, having an energy barrier with an upper bound of $\Delta E^{\ddagger}$ ~ 0.42 eV (~9.7 kcal/mol), a process compatible with the experimental timescales reported in the same work.[64]

4.1.2.3 Octahedral Ru(II) photosensitizers

The pursue of efficient anticancer metallodrugs activated by light absorption is a very active field of research, since the absorption properties of metal-organic complexes usually fall in the visible or infrared region of the spectrum and their chemical, photochemical, and electrochemical properties can be widely tuned through ligand modifications.[54,65,66] In this regard, polypyridyl Ru(II) octahedral complexes play a prominent role due to their rich photophysical and photochemical properties, which can be exploited for both charge- and energy-transfer processes of interest for photobiological applications.[54] In 2022, the photophysics and photochemistry of a series of 2,9-dimethyl-1,10-phenantroline (dmp) thiophene-substituted Ru(II) complexes was studied by using experimental spectroscopy techniques and quantum-chemistry methods.[58] The complexes with either 3 (**3T**) or four (**4T**) thiophene rings attached to the imidazo[4,5-*f*][1,10]-phenantroline ligand showed excellent photobiological properties, exhibiting unprecedented attomolar phototoxicity towards cancer cells in normoxia and picomolar phototoxicity in hypoxia. The QM results identified the population of triplet intra-ligand charge transfer states ^{3}ILCT localized over the thiophene chain after visible light absorption, leading to long-lived triplet lifetimes ranging from 20 to 25 ms.

The triplet decay pathways driven by the Ru-N bonds stretching indicated relatively large energy barriers to decay to the singlet ground state, a finding compatible with the long triplet lifetimes and the low photosubstitution yields measured experimentally.[58] The absence of the methyl groups at the 1,10-phenantroline derivatives decreased the phototoxicity of the series, although the electronic structure properties remain similar, being the ^{3}ILCT the doorway to biological damage also for the **3T** and **4T** derivatives.[66]

4.1.2.4 Os(II)+Pt(II) dyads

Another emergent phototherapy is the so-called photoactivated chemotherapy (PCT), in which the anticancer agent is a chemotherapeutic prodrug which is converted to the active drug after light absorption. The combination of an octahedral Os(II) complex with a cis-platinum derivative Pt(II) and the optical and photochemical properties of this Os(II)-Pt(II) dyad was studied through computational photochemistry tools in 2022.[59] The study employs biased QM/MM dynamics to provide a detailed description of the photoactivation process. This approach allows for the inclusion of both dynamic and environmental effects, offering a comprehensive understanding of the molecular interactions at play.

Os, even though less explored than its group 8 counterpart Ru, offers an extended absorption window, making it particularly advantageous for phototherapy applications. Meanwhile, the platinum component is known for its potent DNA-binding and cytostatic properties. This dual-metal complex is engineered to harness the synergistic effects of both metals, combining the photodynamic properties of Os with the chemotherapeutic efficacy of Pt. The photoactivation of the Pt(II) unit by the Os(II) component represents an unprecedented mechanism in anticancer therapy. Upon light irradiation, the Os(II) moiety undergoes a metal-to-metal charge transfer (^{3}MMCT) state, facilitating the photolabilization of the Pt(II)-Cl bond. This process is critical as it triggers the release of the active Pt(II) species directly at the target site, thereby enhancing its therapeutic efficacy while minimizing systemic toxicity. The free energy profile computed with the umbrella sampling method at the QM/MM level revealed a very small

energy barrier $\Delta E^{\ddagger}$ ~ 3.4 kcal/mol for the triplet state, making the activation of this Os(II)-Pt(II) dyad a very favorable process.[59]

4 Computational Photonanotechnology

4.1 Organic Compounds

The understanding of the excited-state dynamics of conjugated organic materials is of crucial importance for the development of more efficient optoelectronic devices.[67,68] The photophysics of π-conjugated compounds has been extensively studied over the last few decades, with transient absorption (TA) evolving into a powerful tool for analysing complex systems and excited state processes such as the excited-state absorption (ESA).[69–71] However, TA analysis is challenging due to the complex spectral features and time traces, often requiring additional experiments and quantum chemical support for accurate assignment.[72] This is particularly difficult because the first excited singlet state (S_1), from which ESA features at fast delay times originate, usually exhibits a higher degree of electronic correlation compared to the ground state (S_0).[73] Moreover, CI can be much stronger in ESA than in ground-state absorption (GSA), requiring a proper description of higher-order excitations through multiconfigurational methods like the CASPT2, which has been successfully applied to study both GSA and ESA in small-to-medium-sized conjugated compounds.[74–77]

Since CASPT2 is limited to treat about 18 active electrons in 18 molecular orbitals, attempts to calculate ESA features with cost-effective methods, such as TD-DFT, in its linear response and quadratic response (QR-TD-DFT) variations.[71,78,79] The latter is expected to treat well ESA in cases with small higher-order excitation contributions, as demonstrated for low-lying ππ* states in DNA bases.[80,81] More recently, QR-TD-DFT was applied to investigate the ESA features of distyrylbenzene (DSB) (*Figure 7*), one of the working horses of the filed. It was shown for DSB that QR-TD-DFT gives a reasonable agreement with the experimental ESA spectra, concerning excitation energies and oscillator strengths.[71] The reasonable agreement with the ESA experiments, however, raised concerns on the adequacy of the QR-TD-DFT

approach and the relevance of second order CI, thus suggesting a benchmarking of the GSA and ESA spectra for the (rather large) DSB molecule.

In 2022, Roldao *et al.*[82] revisited the DSB ground and excited-state absorption spectra features applying the CASSCF/CASPT2 methodology to investigate the role of higher order excitations. In the case of the GSA spectrum, despite the non-negligible double (and higher) excitation contributions, the CASPT2 general description of the bright $1A_g$ to $1B_u$ transition largely resemble that of TD-DFT (H → L; 73% against H → L, 94%). For the ESA spectrum, however, CASPT2 revealed that double (and higher order) excitations significantly contribute to the formation of most of the allowed A_g states. In particular, the dominating PA_1 band, described by the $1B_u \rightarrow 5A_g$ transition, shows strong double excitation character with 2el.: H → L (20%) as the most prominent contribution, followed by the H → L+1 (15%) and H-1 → L (13%) (against the H → L+1; 71% given by TD-DFT), see *Figure 7*. Such results highlight the relevance of double (and higher order) excitations, in particular for ESA, in agreement with previous studies on other (smaller) molecules.[83–85] The authors argue that the previous good representation for the ESA features of DSB by QR-TD-DFT may be attributed to a number of factors; this includes the parametrization of the hybrid functional used (BHandHLYP), the correlation effects included to some degree in TD-DFT, and the inclusion of some double excitation effects via quadratic response.[78,86]

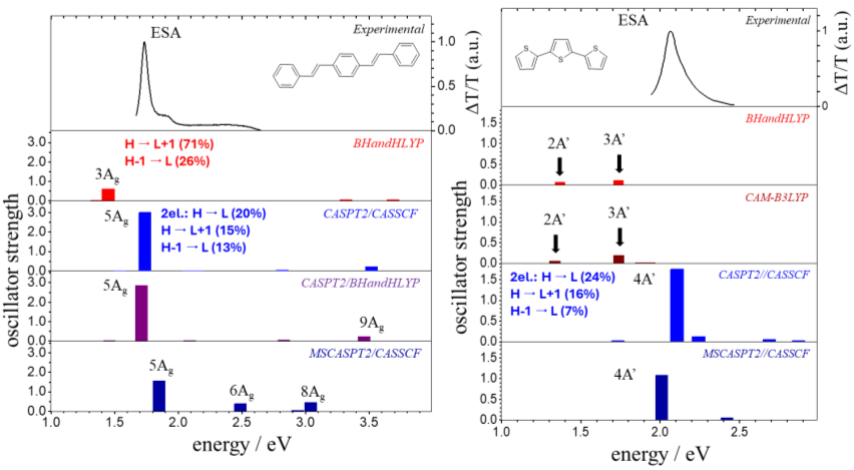

Figure 7 Calculated transitions from S_1 to singlet excited states S_n for DSB (left) and terthiophene (right). Experimental normalised ESA spectra of DSB in dioxane solution from ref [71] *and terthiophene in dioxane solution from ref* [87] *are shown on the top for comparison. Adapted from Figs. 1 and 3 with permissions from Ref.* [88]*. Copyright 2022 American Chemical Society.*

Later in 2022, Roldao *et al*.[88] examined the case of thiophenes, another central family of compounds in the field. The previous success of QR-TD-DFT observed with DSB and stilbene did not hold for thiophenes. The method largely failed even in a qualitative manner, by generating complex ESA spectral patterns, which do not agree with the rather plain experimental features, see *Figure 7*. Similar to the DSB case, a substantial contribution of higher-order excitations (mainly double excitations) was observed in the ESA transitions of thiophenes. For terthiophene, the PA_1 band is assigned to the 1A″ → 4A′ transition. CASPT2 revealed the 2el.: H →L, H → L+1 and H−1 → L excitations as the main contributions to the dominant transition in the ESA spectrum, see *Figure 7*. Molecular orbital analysis revealed an asymmetry in the energy spacing HOMO−1, HOMO vs LUMO, LUMO+1, giving rise to two accessible states with similar oscillator strengths, in contrast to experiment. Longer thiophenes, however, adapt approximately the molecular orbital (MO) scheme for alternant hydrocarbons just like DSB. The authors concluded that the very different DFT description for the two families of compounds, despite of the similar electronic description at the CASPT2 level (and the good agreement with the experiment), can be attributed to such asymmetric MO energy spacing in the case of small thiophene. This is corroborated by the good results obtained with DFT for longer thiophenes. The study with thiophenes concluded that, for "well-behaved" systems (such as stilbene, DSB and large thiophenes), QR-TD-DFT provides a reasonable representation of the ESA features despite its incomplete electronic description due to rather small energy shifts by higher-order excitations. The authors emphasise, however, the importance of careful MO analysis to decide for the DFT approach.

CASPT2 revealed a more complex electronic situation for ESA as compared to GSA. For ESA, double and higher-order excitations play a relevant role for most of the state CI description. The pointed crucial importance of double and higher order excitations in the ESA spectra of π-conjugated molecules, demonstrate the necessity of a CASPT2 detailed treatment for these types of electronic structure problems and molecular systems. Preliminary computations at CI with single and double excitations (CISD) or TD-DFT (in a future implementation of double hybrid functionals for ESA) may be used to identify cases with strong multiconfigurational character. Spin-flip TD-DFT methods, including the mixed-reference spin-flip TD-DFT approach, promises an enhanced description of double excitations by incorporating numerous electronic configurations, all at the computational cost of a linear response TD-DFT calculation.[89] Nevertheless, more detailed studies are needed to evaluate the capabilities of such implementations. For CASPT2, time consumption, truncation of the active space, and selection of the MOs are, issues which limit the general applicability of the method. The use of density matrix renormalization group (DMRG) as an active space solver with CASPT2 is a promising possibility, although currently it still requires efficient and well-tested implementations.[90,91]

4.2 Inorganic Compounds

Ionic transition metal complexes (iTMCs), mainly based on Ir(III), are widely investigated for many applications such as light emitting electrochemical cells (LECs) devices.[92] To obtain a feasible LECs device, iTMCs complexes with a high emission quantum yield (Φ_{em}) are desired. For this reason, it is necessary to understand all the radiative and non-radiative decays paths that govern the phosphorescence emission for these iTMCs. The kinetic model[93,94] to study Φ_{em} relies on the calculation of three main processes (see *Figure 8*), characterised by their respective rate constants (k_{rad}, k_{ISC}, and k_{nr}). The first one (k_{rad}) is the direct phosphorescence from the triplet emitting excited state (T_1) to the singlet ground state (S_0). This T_1 state can present different nature, for instance metal to ligand charge transfer (^{3}MLCT) or ligand-centered (^{3}LC) between others. The second one (k_{ISC}, or "temperature-independent non-

radiative decay") is the direct non-radiative decay from the T_1 to the S_0 state. The third one (k_{nr}), is the temperature dependent non-radiative decay path through the triplet metal-centered states (^{3}MC). These ^{3}MC states are characterised by a $t_{2g} \rightarrow e_g^*$ electronic transition, leading to a strong geometrical distortion and consequently the destabilization of the energy of the S_0 state. Once a ^{3}MC state is populated, two different processes are possible: either coming back to the T_1 state or reaching an accessible minimum energy crossing point (MECP) between the T_1 and S_0 states, promoting an efficient non-radiative decay to the latter state. It is clear that for electroluminescence applications the main aim is to look for iTMCs with high k_{rad} and small k_{ISC}, and k_{nr}. In this sense, DFT and TD-DFT calculations have shown its usefulness, in the last two years, elucidating the main radiative and/or non-radiative decay paths for a several iTMCs based on Ir(III) or Ru(II).[95–104]

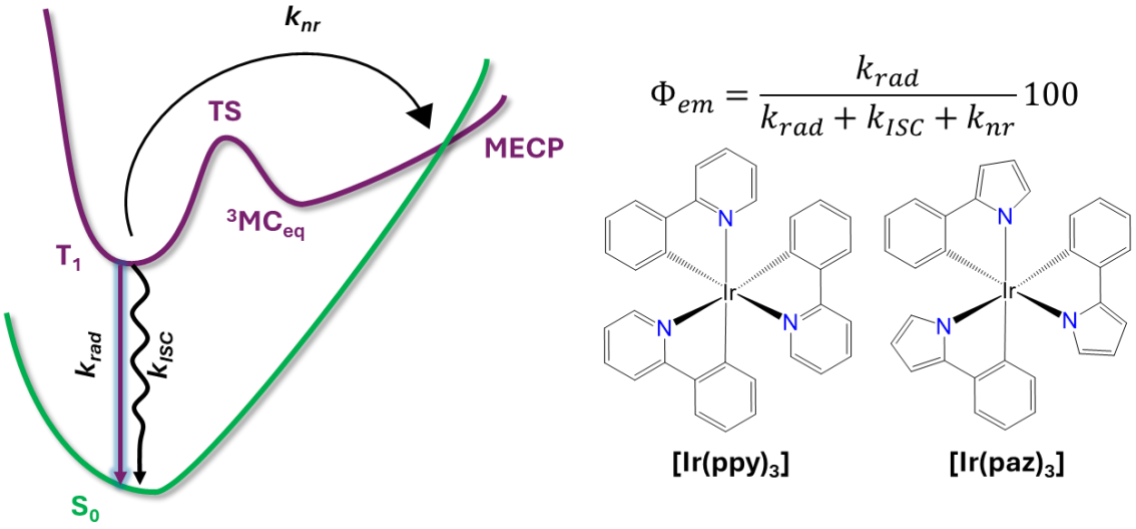

Figure 8 Schematic representation of the kinetic model employed for the photophysics for two reference [Ir(C^N)$_3$] complexes.

Tang, Hu and coworkers,[105] studied a family of Ir(III) complexes based on the general formula [Ir(C^N)$_3$],where the C^N ligand is based on phenyl-azole. In their work, they studied how the k_{rad}, k_{ISC}, and k_{nr} rate constant are affected introducing different heteroatoms (N, O, S) in the

azole ring. Performing quadratic response theory to calculate the k_{rad}, they showed that introducing O or S atoms in the azole ring, leads to a lower k_{rad} rate constant. They justify this result due to the lower ^{3}MLCT character of the T_1 emitting state. Nevertheless, the authors also pointed out that increasing the ^{3}MLCT character not only increased the k_{rad} but also the k_{ISC} rate constant, as the two rate constants depend directly on the SOC.[106] The decrease of k_{ISC} is however not enough to compensate the decrease in k_{rad}, so globally these substitutions determine a decrease of the emission quantum yield. A second modification that was study is the substitution of C atoms with N, analyzing in this case also the change in the recombination energy (λ), important for the k_{ISC} process. The introduction of N atoms promotes the ^{3}MLCT character of the emitting state and thus increasing the k_{rad}, while λ decreases making the k_{ISC} less relevant than the k_{rad}, improving the overall performance of the Ir(III) complexes. The k_{nr} processes were also studied showing two main conclusions. The first one, and in agreement with other theoretical studies, is that the limiting step is the population of the ^{3}MC state as the energy barrier between the MECP and ^{3}MC state minimum is always lower than 1 kcal/mol. The second one, is that the energy barriers to populate the ^{3}MC state from the T_1 state through the corresponding transition state (TS) are around 6-13 kcal/mol depending to the nature of the emitting state (^{3}MLCT states present lower energy barriers than ^{3}LC states). The authors postulate that this difference in the barriers, could be produced due to the different strengths of the coordinate bonds between the ^{3}MLCT and ^{3}LC states.

Luo and coworkers,[107] also analysed the effect of the N-substitution and the Br substitution in another [Ir(C^N)$_3$] family of complexes on the k_{nr} decay process employing thermal vibration correlation function formalism.[108] In this case the C^N ligands are based on phenyl-pyridine. They concluded that the N-substitution on the phenyl rings can lead to different results in the final k_{nr} depending on its influence on SOC and the energy barriers to populate the ^{3}MC states. On the other hand, the N-substitution on the pyridine generally increased the energy barrier and the spin-orbit coupling (SOC), but the increased energy barrier effect was more significant, leading to a reduction (up to 3 times) in the k_{nr} decay rate constant. In order to study the heavy

atom effect, they substituted one hydrogen atom on the phenyl or pyridine rings with a Br atom. They found that both substitutions provided higher energy barriers to populate the ^{3}MC states leading to smaller k_{nr} decay rate constant. However, the substitution on the pyridine ring provides an almost two-times higher energy barrier to populate such ^{3}MC state, than when the Br is introduced in the phenyl ring.

To conclude on this topic, during 2022 and 2023, significant efforts have been made to reproduce and predict the experimental radiative and non-radiative decay processes in iTMCs. These two works are only a small example of how computational chemistry has been proved as a reliable and feasible way to study all the different radiative and non-radiative decay processes, and their relative importance, for iTMCs complexes.

5 Computational Atmospheric Photochemistry

The study of photochemical reactions involving atmospheric compounds is an essential area of research within the atmospheric chemistry and modelling field. Light-induced processes such as photodissociations can have a major impact on chemical conversions in the atmosphere.[109–111] Thus, analysing the photochemistry of atmospheric molecules is crucial to obtain a comprehensive understanding of the complex reactive networks that govern their lifetime and fate. Theoretical and computational photochemistry can be used to study the excited-state reactivity of atmospheric compounds. A commonly used approach is to perform excited-state dynamics simulations, being trajectory surface hopping[112] among one of the most popular methods.[113,114] These simulations allow for the identification of different photochemical reactions and non-radiative deactivation pathways, the quantification of the corresponding photoproducts and quantum yields, as well as the rationalization of the mechanisms underlying the observed excited-state pathways, especially when combined with a thorough exploration of the PESs of the states involved by means of static calculations.

Within the period revised in this chapter (2022-2023), trajectory surface hopping simulations have been employed to study the photochemistry of species of atmospheric interest including, for example, volatile organic compounds such as 2-hydroperoxypropanal,[115] CF_3COCl,[116] pyruvic acid[117] or methylhydroperoxide,[118] Criegee intermediates formed from the ozonolysis of isoprene,[119–121] as well as a fluorinated[122] and acetone oxide intermediate,[123] and atmospheric mercury compounds relevant to the stratospheric mercury cycle.[124] These studies employ MQC methods such as state-average (SA-)CASSCF or XMS-CASPT2 to describe the electronic structure of the system under study during the simulations, to characterize the studied pathways through static calculations, or for calibration of more computationally efficient levels of theory based on single-reference methods.

Similarly, in a recent study by Francés-Monerris and co-workers, *ab initio* non-adiabatic molecular dynamics simulations using the surface hopping including arbitrary couplings (SHARC)[125] approach were carried out to study the photochemistry of several $^1(SO)_2$ isomers relevant to the understanding of the composition and the reported near UV absorption of the Venusian atmosphere (mainly within the 320-400 nm wavelength range).[126–128] The *cis*-OSSO and *trans*-OSSO isomers have been proposed as potential molecular candidates to be the so-called “unknown UV-absorber(s)” responsible for such reported near UV absorption.[126,129,130] Concerning their photochemical reactivity, after light absorption in the near-UV range both *cis*-OSSO and *trans*-OSSO are suggested to mainly generate ^{3}SO based on *ab-initio* calculations made by Frandsen and co-workers[131]. However, in a recent modelling study by Pinto and co-workers, in which they analyse the role of $^3(SO)_2$ dimers in the generation of polysulfur (S_n), also proposed as candidates accounting for the reported near-UV absorption, and polysulfur oxides (S_nO) on the atmosphere of Venus,[132] the authors considered the following light-induced reactivity for *cis*-OSSO:

$$^1\text{cis-OSSO} + h\upsilon \rightarrow {}^3S_2 + {}^3O_2$$

The formed $^3S_2$ could yield polysulfur S_n species through self-propagation polymerizations. This light-induced process was proposed based on the results reported in the study of Wu and co-workers in which they analysed the photoconversions of a set of $^1(SO)_2$ isomers condensed on a cryogenic N_2-matrix from gaseous ^3SO followed by UV-Vis spectroscopy, ascribing the reduction and increase of different absorption bands due to the generation and depletion of the species involved.[133] More specifically, after irradiation by 365 nm light, the 375 nm band, associated with *cis*-OSSO, was depleted,along with a simultaneous increase of a band at 287 nm assigned to $^3S_2$. However, the authors suggest other possible decomposition products related to such absorption. Moreover, a posterior study by Frandsen and co-workers, based on computed absorption spectra of the isomers above-mentioned, suggested that cis-OSSO may only account for the part of the absorption band at < 360 nm.[130] The other part at lower energies is likely to be originated by trans- OSSO considering their simulated spectra for this isomer.[130]

Considering the uncertainties surrounding this photochemical generation of $^3S_2$ from *cis*-OSSO photodissociation, Francés-Monerris and co-workers analysed the gas-phase light-induced reactivity of both *cis*-OSSO and *trans*-OSSO by means of SHARC dynamics in combination with the MS-CASPT2 method. After excitation in the atmospherically relevant window (310-496 nm), populating primarily their second singlet excited state, both systems photodissociate in less than 140 fs generating only ^3SO + ^3SO (Figure 9a and b). The quantum yields obtained were 95% and 90% for *cis*-OSSO and *trans*-OSSO, respectively, taking into account that the remaining 5% and 10% of trajectories did not lead to photodissociation within the considered simulation time. However, these non-reactive trajectories showed an evolution that could lead to non-reactive decays or cause photoisomerizations. The predominance of the ^3SO + ^3SO photoproduct is in agreement with previous theoretical assessments by Frandsen and co-workers[129] and rules out the proposal of $^3S_2$ as a possible photoproduct of *cis*-OSSO photolysis. Thus, this photolytic pathway cannot represent a relevant source of polysulfur in Venus.

Additionally, excited-state dynamics simulations were carried out for other isomers (i.e, cyclic-OS(=O)S, trigonal S=SO_2, *cis*-OSOS and *trans*-OSOS) using TD-DFT for the description of the electronic structure, calibrated with MS-CASPT2 dynamics and static profiles. The results obtained indicate that the photolysis of these isomers generates mainly ^{3}SO fragments and ^{3}S atoms (Figure 9c-f). These results also suggest that a possible pathway to $^3S_2$ could be the recombination of ^{3}S atoms produced from the photodissociation of $^1(SO)_2$, although this recombination is found to be less efficient than ^{3}S oxidation by $^3O_2$.

The significant production of ^{3}SO in the simulations also motivated the authors to explore, by means of MS-CASPT2 calculations, ground-state reactions that could represent an alternative path to $^3S_2$ formation involving the ^{3}SO fragment, *cis*-OSSO, and other species (i.e., NO, O, S, H, ClS), updating previous estimations and confirming that the photochemical reactivity of *cis*-OSSO is faster than its thermal reactivity as assessed by Frandsen and co-workers[131].

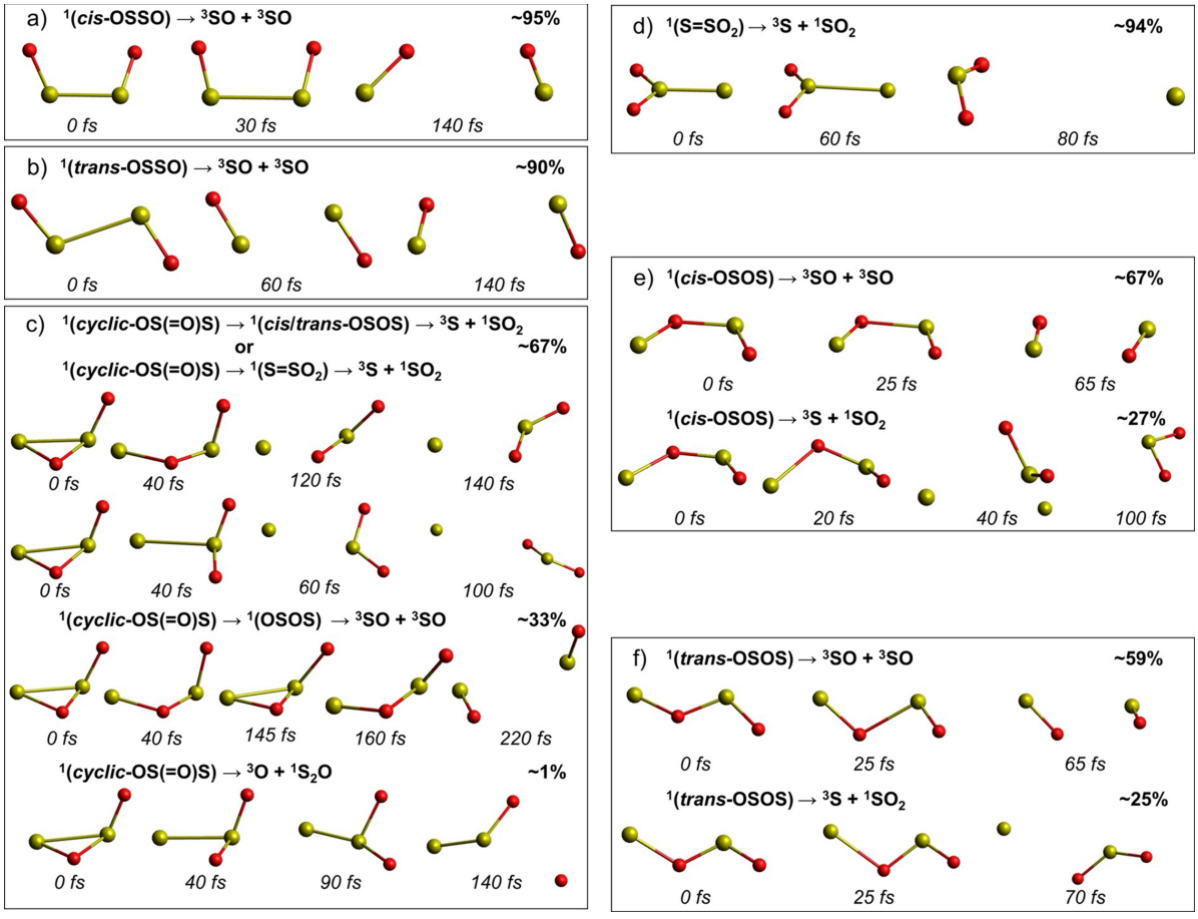

Figure 9 Summary of the different photodissociation pathways and photoproducts ratio obtained for the studied $^{1}(SO)_2$ isomers by means of non-adiabatic molecular dynamics simulations. The spin multiplicity of the photoproducts corresponds to their respective ground-state, assumed to be reached at the end of the photodissociation process. Figure adapted from Ref. [134] *under the Creative Commons BY 4.0 License terms.*

Using photochemical steady state calculations combining the high-level *ab-initio* results obtained and previously reported rates of sulphur reactions, the abundances of selected sulphur species in the Venusian atmosphere were estimated. Summarizing, it was found that the reaction of $^{1}S_2O$ and ^{3}SO to yield $^{3}S_2$ and $^{1}SO_2$ could represent a significant pathway to $^{3}S_2$ formation, obtaining a peak abundance of such species comparable with the values from Pinto and co-workers[132] for the highest rate constant considered (based on the obtained *ab-initio* results) but with a narrower vertical distribution, without considering the unlikely photochemical generation of $^{3}S_2$ from *cis*-OSSO photolysis.

6 Brief overview

To summarise on this revision of articles on computational photochemistry published during 2022 and 2023, we can say that significant efforts have been made in three directions: (i) developing and implementing fast and more reliable methodologies to address studies in the field in software packages like OpenMolcas, (ii) reproducing and providing a rationale of the experimental radiative and non-radiative decay processes, and (iii) providing new knowledge on the electronic and nuclear structure features that determine photo-properties of chromophores of interest in biology, biomedicine, nanotechnology and atmospheric chemistry. The highlighted works in this revision are only representative examples of how computational photochemistry continues demonstrating that it is a reliable and feasible way to study all the different radiative and non-radiative decay processes, and their relative importance in chromophores of small to medium molecular size. Future steps shall be taken towards

achieving the same accuracy in macromolecular systems, which are still challenging in particular in the study of excited state chemistry.

ABBREVIATIONS

3T	3-Thiophene-rings complex
4T	4-Thiophene-rings complex
CAS	Complete Active Space
CASSCF	Complete Active Space Self-Consistent Field
CASPT2	Complete Active Space Second-Order Perturbation Theory
CD-RASPT2	Cholesky Decomposition-based RASPT2
CI	Conical Intersections
CISD	CI with Single and Double excitations
CPD	Cyclobutane Pyrimidine Dimer
DFT	Density Functional Theory
Dmp	2,9-dimethyl-1,10-phenantroline
DMRG	Density Matrix Renormalization Group
DNA	Deoxyribonucleic Acid
DSB	Distyrylbenzene
ESA	Excited-State Absorption
FNO	Frozen Natural Orbital
FNO-CASPT2	Frozen Natural Orbital Complete Active Space Second-Order Perturbation Theory

G	Guanine
GEM	Gemcitabine
GMM	Gaussian Mixture Models
GSA	Ground-State Absorption
HPLC	High-Performance Liquid Chromatography
ICL	Interstrand Cross-Link
ILCT	Intra-Ligand Charge Transfer States
ISC	Intersystem Crossing
iTMC	Ionic Transition Metal Complex
LC	Ligand-Centered
LEC	Light-Emitting Electrochemical Cell
MBPT	Many-Body Perturbation Theory
MC	Metal-Centered
MC-PDFT	Multiconfiguration Pair-Density Functional Theory
MD	Molecular
MECP	Minimum Energy Crossing Point
ML	Machine Learning
MLCT	Metal to Ligand Charge Transfer
MM	Molecular Mechanics
MMCT	Metal-To-Metal Charge Transfer
MO	Molecular Orbital

MQC	Multiconfigurational Quantum Chemistry
MS-CASPT2	Multistate CASPT2
NEA	Nuclear Ensemble Approach
NO	Nitric Oxide
OG	8-oxoguanine
PCT	Photoactivated Chemotherapy
PDT	Photodynamic Therapy
PES	Potential Energy Surface
PSB-11	Protonated Schiff Base 11
PT2	Second-order Perturbation Theory
QM	Quantum Mechanics
QM/MM	Quantum Mechanics/Molecular Mechanics
QR-TD-DFT	Quadratic Response Time Dependent DFT
RAS	Restricted Active Space
RASPT2	Restricted Active Space Second-order Perturbation Theory
RMS-CASPT2	Rotated Multistate CASPT2
ROS	Reactive Oxygen Species
SOC	Spin-Orbit Coupling
T	Thymine
TA	Transient Absorption
TD-DFT	Time-Dependent DFT

TS	Transition State
UV	Ultraviolet
VTP	Verteporfin
XDW-CASPT2	Extended Dynamically Weighted CASPT2
XMS-CASPT2	Extended Multistate

ACKNOWLEDGEMENTS

Research funded by the Projects PID2021-127554NA-I00, PID2021-128490NA-I00 and PID2021-127199NB-I00 funded by the Spanish Ministry of Science and Innovation (MCIN/AEI/10.13039/501100011033) and by "ERDF A way of making Europe.", and the Project CIAICO/2022/121 funded by the Generalitat Valenciana. A.M.A.A. is grateful to the Generalitat Valenciana and the European Social Fund for the predoctoral Contract No. CIACIF/2021/391. The project that gave rise to these results received the support of a fellowship for J.C.-G. from "la Caixa" Foundation (ID 100010434). The fellowship code is LCF/BQ/DR20/11790027. M.N.-M. acknowledges Universitat de València for the predoctoral grant "Atracció de Talent 2020". J.C.-Z. is thankful for the Grant PRE2022-101260 funded by MCIN/AEI/10.13039/501100011033 and "ESF Investing in your future". J.C.R. is grateful to Generalitat Valenciana (postdoctoral contract APOSTD/2022/027) for financial support. A. B.-S. is grateful to Generalitat Valenciana (postdoctoral contract APOSTD/2022/029) for financial support. I. S.-D. thanks Generalitat Valenciana (Conselleria d'Educació, Universitats i Ocupació) for his predoctoral grant CIACIF/2021/438".

References

1 ISI Web of Knowledge, Thomson Reuters, http://wokinfo.com.

2 G. Li Manni, I. Fdez. Galván, A. Alavi, F. Aleotti, F. Aquilante, J. Autschbach, D. Avagliano, A. Baiardi, J. J. Bao, S. Battaglia, L. Birnoschi, A. Blanco-González, S. I. Bokarev, R. Broer, R. Cacciari, P. B. Calio, R. K. Carlson, R. Carvalho Couto, L. Cerdán, L. F. Chibotaru, N. F. Chilton, J. R. Church, I. Conti, S. Coriani, J. Cuéllar-Zuquin, R. E. Daoud, N. Dattani, P. Decleva, C. de Graaf, M. G. Delcey, L. De Vico, W. Dobrautz, S. S. Dong, R. Feng, N. Ferré, M. Filatov, L.

Gagliardi, M. Garavelli, L. González, Y. Guan, M. Guo, M. R. Hennefarth, M. R. Hermes, C. E. Hoyer, M. Huix-Rotllant, V. K. Jaiswal, A. Kaiser, D. S. Kaliakin, M. Khamesian, D. S. King, V. Kochetov, M. Krośnicki, A. A. Kumaar, E. D. Larsson, S. Lehtola, M. B. Lepetit, H. Lischka, P. López Ríos, M. Lundberg, D. Ma, S. Mai, P. Marquetand, I. C. D. Merritt, F. Montorsi, M. Mörchen, A. Nenov, V. H. A. Nguyen, Y. Nishimoto, M. S. Oakley, M. Olivucci, M. Oppel, D. Padula, R. Pandharkar, Q. M. Phung, F. Plasser, G. Raggi, E. Rebolini, M. Reiher, I. Rivalta, D. Roca-Sanjuán, T. Romig, A. A. Safari, A. Sánchez-Mansilla, A. M. Sand, I. Schapiro, T. R. Scott, J. Segarra-Martí, F. Segatta, D. C. Sergentu, P. Sharma, R. Shepard, Y. Shu, J. K. Staab, T. P. Straatsma, L. K. Sørensen, B. N. C. Tenorio, D. G. Truhlar, L. Ungur, M. Vacher, V. Veryazov, T. A. Voß, O. Weser, D. Wu, X. Yang, D. Yarkony, C. Zhou, J. P. Zobel and R. Lindh, *J Chem Theory Comput*, 2023, **19**, 6933.

3 F. Neese, *Wiley Interdiscip Rev Comput Mol Sci*, 2022, **12**, e1606.

4 T. Shiozaki, *Wiley Interdiscip Rev Comput Mol Sci*, 2018, **8**, e1331.

5 S. Battaglia and R. Lindh, *J Chem Theory Comput*, 2020, **16**, 1555.

6 S. Battaglia and R. Lindh, *Journal of Chemical Physics*, 2021, **154**, 34102.

7 J. Finley, P. Å. Malmqvist, B. O. Roos and L. Serrano-Andrés, *Chem Phys Lett*, 1998, **288**, 299.

8 T. Shiozaki, C. Woywod and H. J. Werner, *Physical Chemistry Chemical Physics*, 2012, **15**, 262.

9 F. Aquilante, T. K. Todorova, L. Gagliardi, T. B. Pedersen and B. O. Roos, *Journal of Chemical Physics*, 2009, **131**, 034113.

10 J. Segarra-Martí, M. Garavelli and F. Aquilante, *J Chem Theory Comput*, 2015, **11**, 3772.

11 S. Battaglia, L. Fransén, I. Fdez. Galván and R. Lindh, *J Chem Theory Comput*, 2022, **18**, 4814.

12 N. Forsberg and P. Å. Malmqvist, *Chem Phys Lett*, 1997, **274**, 196.

13 V. Sauri, L. Serrano-Andrés, A. R. M. Shahi, L. Gagliardi, S. Vancoillie and K. Pierloot, *J Chem Theory Comput*, 2011, **7**, 153.

14 G. Li Manni, R. K. Carlson, S. Luo, D. Ma, J. Olsen, D. G. Truhlar and L. Gagliardi, *J Chem Theory Comput*, 2014, **10**, 3669.

15 C. Zhou, M. R. Hermes, D. Wu, J. J. Bao, R. Pandharkar, D. S. King, D. Zhang, T. R. Scott, A. O. Lykhin, L. Gagliardi and D. G. Truhlar, *Chem Sci*, 2022, **13**, 7685.

16 R. Pandharkar, M. R. Hermes, D. G. Truhlar and L. Gagliardi, *Journal of Physical Chemistry Letters*, 2020, **11**, 10158.

17 D. Presti, J. Kadlec, D. G. Truhlar and L. Gagliardi, *Theor Chem Acc*, 2020, **139**, 1.

18 S. J. Stoneburner, D. G. Truhlar and L. Gagliardi, *J Phys Chem A*, 2020, **124**, 1187.

19 A. M. Sand, C. E. Hoyer, K. Sharkas, K. M. Kidder, R. Lindh, D. G. Truhlar and L. Gagliardi, *J Chem Theory Comput*, 2018, **14**, 126.

20 T. R. Scott, M. R. Hermes, A. M. Sand, M. S. Oakley, D. G. Truhlar and L. Gagliardi, *Journal of Chemical Physics*, 2020, **153**, 014106.

21 T. R. Scott, M. S. Oakley, M. R. Hermes, A. M. Sand, R. Lindh, D. G. Truhlar and L. Gagliardi, *Journal of Chemical Physics*, 2021, **154**, 074108.

22 J. J. Bao, M. R. Hermes, T. R. Scott, A. M. Sand, R. Lindh, L. Gagliardi and D. G. Truhlar, *Mol Phys*, 2022, **120**, e2110534.

23 S. Mai, D. Avagliano, M. Heindl, P. Marquetand, M. F. S. Menger, M. Oppel, F. Plasser, S. Polonius, M. Ruckenbauer, Y. Shu, D. G. Truhlar, L. Zhang, P. Zobel and L. González, *Zenodo*, 2023, 10.5281/zenodo.7828641.

24 S. Mai, P. Marquetand and L. González, *Wiley Interdiscip Rev Comput Mol Sci*, 2018, **8**, e1370.

25 O. Weingart, A. Nenov, P. Altoè, I. Rivalta, J. Segarra-Martí, I. Dokukina and M. Garavelli, *Journal of Molecular Modeling 2018 24:9*, 2018, **24**, 1.

26 QCEXVAL group. MULTISPEC repository on GitHub.

27 R. Crespo-Otero and M. Barbatti, *Theor Chem Acc*, 2012, **131**, 1.

28 L. Cerdán and D. Roca-Sanjuán, *J Chem Theory Comput*, 2022, **18**, 38.

29 J. Cuéllar-Zuquin, A. Giussani and J. Segarra-Martí, in *Theoretical and Computational Photochemistry: Fundamentals, Methods, Applications and Synergy with Experimental Approaches*, Elsevier, 2023, p. 417.

30 A. A. Beckstead, Y. Zhang, M. S. De Vries and B. Kohler, *Physical Chemistry Chemical Physics*, 2016, **18**, 24228.

31 S. Boldissar and M. S. De Vries, *Physical Chemistry Chemical Physics*, 2018, **20**, 9701.

32 L. Serrano-Andrés and M. Merchán, *Journal of Photochemistry and Photobiology C: Photochemistry Reviews*, 2009, **10**, 21.

33 M. Ben-Nun, F. Molnar, K. Schulten and T. J. Martínez, *Proc Natl Acad Sci U S A*, 2002, **99**, 1769.

34 J. S. Lim and S. K. Kim, *Nat Chem*, 2010, **2**, 627.

35 M. Kowalewski, K. Bennett, K. E. Dorfman and S. Mukamel, *Phys Rev Lett*, 2015, **115**, 193003.

36 D. Polli, P. Altoè, O. Weingart, K. M. Spillane, C. Manzoni, D. Brida, G. Tomasello, G. Orlandi, P. Kukura, R. A. Mathies, M. Garavelli and G. Cerullo, *Nature*, 2010, **467**, 440.

37 J. Cuéllar-Zuquin, A. J. Pepino, I. Fdez. Galván, I. Rivalta, F. Aquilante, M. Garavelli, R. Lindh and J. Segarra-Martí, *J Chem Theory Comput*, 2023, **19**, 8258.

38 G. J. Atchity, S. S. Xantheas and K. Ruedenberg, *J Chem Phys*, 1991, **95**, 1862.

39 R. Improta, F. Santoro and L. Blancafort, *Chem Rev*, 2016, **116**, 3540.

40 R. Borrego-Varillas, A. Nenov, P. Kabaciński, I. Conti, L. Ganzer, A. Oriana, V. K. Jaiswal, I. Delfino, O. Weingart, C. Manzoni, I. Rivalta, M. Garavelli and G. Cerullo, *Nature Communications 2021 12:1*, 2021, **12**, 1.

41 M. Merchán, R. González-Luque, T. Climent, L. Serrano-Andrés, E. Rodríguez, M. Reguero and D. Peláez, *Journal of Physical Chemistry B*, 2006, **110**, 26471.

42 A. J. Pepino, J. Segarra-Martí, A. Nenov, R. Improta and M. Garavelli, *Journal of Physical Chemistry Letters*, 2017, **8**, 1777.

43 M. Boggio-Pasqua, M. A. Robb and M. J. Bearpark, *Journal of Physical Chemistry A*, 2005, **109**, 8849.

44 K. F. Hall, M. Boggio-Pasqua, M. J. Bearpark and M. A. Robb, *Journal of Physical Chemistry A*, 2006, **110**, 13591.

45 A. M. Tokmachev, M. Boggio-Pasqua, M. J. Bearpark and M. A. Robb, *Journal of Physical Chemistry A*, 2008, **112**, 10881.

46 G. M. Rodríguez-Muñiz, A. B. Fraga-Timiraos, M. Navarrete-Miguel, A. Borrego-Sánchez, D. Roca-Sanjuán, M. A. Miranda and V. Lhiaubet-Vallet, *Journal of Organic Chemistry*, 2023, **88**, 10111–10121.

47 R. R. Allison and K. Moghissi, *Photodiagnosis Photodyn Ther*, 2013, **10**, 331.

48 D. E. J. G. J. Dolmans, D. Fukumura and R. K. Jain, *Nat Rev Cancer*, 2003, **3**, 380.

49 R. Falk-Mahapatra and S. O. Gollnick, *Photochem Photobiol*, 2020, **96**, 550.

50 A. Fraix, C. Parisi, M. Seggio and S. Sortino, *Chemistry – A European Journal*, 2021, **27**, 12714.

51 S. Sortino, *Chem Soc Rev*, 2010, **39**, 2903.

52 M. E. Alberto, N. Russo and C. Adamo, *Chemistry – A European Journal*, 2016, **22**, 9162.

53 M. E. Alberto, J. Pirillo, N. Russo and C. Adamo, *Inorg Chem*, 2016, **55**, 11185.

54 S. Monro, K. L. Colón, H. Yin, J. Roque, P. Konda, S. Gujar, R. P. Thummel, L. Lilge, C. G. Cameron and S. A. McFarland, *Chem Rev*, 2019, **119**, 797.

55 R. Alzeibak, T. A. Mishchenko, N. Y. Shilyagina, I. V. Balalaeva, M. V. Vedunova and D. V. Krysko, *J Immunother Cancer*, 2021, **9**, e001926.

56 C. Mari, V. Pierroz, S. Ferrari and G. Gasser, *Chem Sci*, 2015, **6**, 2660.

57 A. Francés-Monerris, I. Tuñón and A. Monari, *J Phys Chem Lett*, 2019, **10**, 6750.

58 J. Roque III, H. Cole, P. Barrett, L. Lifshits, R. Hodges, S. Kim, A. Francés-Monerris, M. E. Alberto, C. Cameron and S. McFarland, *J Am Chem Soc*, 2022, **144**, 8317.

59 M. E. Alberto and A. Francés-Monerris, *Physical Chemistry Chemical Physics*, 2022, **24**, 19584.

60 A. M. A. Abdelgawwad, D. Roca-Sanjuán and A. Francés-Monerris, *J Chem Phys*, 2023, **159**, 224106.

61 E. Moysan, G. Bastiat and J.-P. Benoit, *Mol Pharm*, 2013, **10**, 430.

62 Y. Han, W. Chen, Y. Kuang, H. Sun, Z. Wang and X. Peng, *Chem Res Toxicol*, 2015, **28**, 919–926.

63 A. M. A. Abdelgawwad, A. Monari, I. Tuñón and A. Francés-Monerris, *J Chem Inf Model*, 2022, **62**, 3239.

64 A. Fraix, C. Parisi, G. Longobardi, C. Conte, A. Pastore, M. Stornaiuolo, A. C. E. Graziano, M. E. Alberto, A. Francés-Monerris, F. Quaglia and S. Sortino, *Biomacromolecules*, 2023, **24**, 3887.

65 L. M. Loftus, K. F. Al-Afyouni and C. Turro, *Chemistry–A European Journal*, 2018, **24**, 11550.

66 H. D. Cole, A. Vali, J. A. I. I. I. Roque, G. Shi, G. Kaur, R. O. Hodges, A. Francés-Monerris, M. E. Alberto, C. G. Cameron and S. A. McFarland, *Inorg Chem*, 2023, **62**, 21181.

67 J. Gierschner, J. Shi, B. Milián-Medina, D. Roca-Sanjuán, S. Varghese and S. Y. Park, *Adv Opt Mater*, 2021, **9**, 2002251.

68 S. C. Rasmussen, S. J. Evenson and C. B. McCausland, *Chemical Communications*, 2015, **51**, 4528.

69 G. Lanzani, G. Cerullo, S. Stagira and S. De Silvestri, *J Photochem Photobiol A Chem*, 2001, **144**, 13.

70 G. Ginocchietti, E. Cecchetto, L. De Cola, U. Mazzucato and A. Spalletti, *Chem Phys*, 2008, **352**, 28.

71 E. F. Oliveira, J. Shi, F. C. Lavarda, L. Lüer, B. Milián-Medina and J. Gierschner, *Journal of Chemical Physics*, 2017, **147**, 034903.

72 J. R. Ochsmann, D. Chandran, D. W. Gehrig, H. Anwar, P. K. Madathil, K. S. Lee and F. Laquai, *Macromol Rapid Commun*, 2015, **36**, 1122.

73 L. Serrano-Andrés and M. Merchán, *Journal of Molecular Structure: THEOCHEM*, 2005, **729**, 99–108.

74 M. A. Izquierdo, J. Shi, S. Oh, S. Y. Park, B. Milián-Medina, J. Gierschner and D. Roca-Sanjuán, *Physical Chemistry Chemical Physics*, 2019, **21**, 22429.

75 M. Rubio, M. Merchán, R. Pou-Amérigo and E. Ortí, *ChemPhysChem*, 2003, **4**, 1308.

76 A. Prlj, B. F. E. Curchod and C. Corminboeuf, *Physical Chemistry Chemical Physics*, 2015, **17**, 14719.

77 V. Molina, M. Merchán and B. O. Roos, *Journal of Physical Chemistry A*, 1997, **101**, 3478.

78 P. Elliott, S. Goldson, C. Canahui and N. T. Maitra, *Chem Phys*, 2011, **391**, 110.

79 R. B. Roseli, P. C. Tapping and T. W. Kee, *Journal of Physical Chemistry Letters*, 2017, **8**, 2806.

80 D. A. Fedotov, A. C. Paul, H. Koch, F. Santoro, S. Coriani and R. Improta, *ChemRxiv*, 2021, preprint, DOI:10.26434/chemrxiv-2021-3hwfv.

81 V. K. Jaiswal, J. Segarra-Martí, M. Marazzi, E. Zvereva, X. Assfeld, A. Monari, M. Garavelli and I. Rivalta, *Physical Chemistry Chemical Physics*, 2020, **22**, 15496.

82 J. C. Roldao, E. F. Oliveira, B. Milián-Medina, J. Gierschner and D. Roca-Sanjuán, *Journal of Chemical Physics*, 2022, **156**, 044102.

83 A. Giussani, J. Segarra-Martí, A. Nenov, I. Rivalta, A. Tolomelli, S. Mukamel and M. Garavelli, *Theor Chem Acc*, 2016, **135**, 121.

84 J. Segarra-Martí, A. J. Pepino, A. Nenov, S. Mukamel, M. Garavelli and I. Rivalta, *Theor Chem Acc*, 2018, **137**, 47.

85 A. Nenov, A. Giussani, J. Segarra-Martí, V. K. Jaiswal, I. Rivalta, G. Cerullo, S. Mukamel and M. Garavelli, *Journal of Chemical Physics*, 2015, **142**, 212443.

86 S. M. Parker, D. Rappoport and F. Furche, *J Chem Theory Comput*, 2018, **14**, 807.

87 D. Grebner, M. Helbig and S. Rentsch, *Journal of Physical Chemistry*, 1995, **99**, 16991.

88 J. C. Roldao, E. F. Oliveira, B. Milián-Medina, J. Gierschner and D. Roca-Sanjuán, *J Chem Theory Comput*, 2022, **18**, 5449.

89 W. Park, K. Komarov, S. Lee and C. H. Choi, *Journal of Physical Chemistry Letters*, 2023, **14**, 8896.

90 A. Baiardi and M. Reiher, *J Chem Phys*, 2020, **152**, 040903.

91 S. Keller, M. Dolfi, M. Troyer and M. Reiher, *J Chem Phys*, 2015, **143**, 244118.

92 R. D. Costa, E. Ortí, H. J. Bolink, F. Monti, G. Accorsi and N. Armaroli, *Angewandte Chemie International Edition*, 2012, **51**, 8178.

93 X. Zhang, D. Jacquemin, Q. Peng, Z. Shuai and D. Escudero, *Journal of Physical Chemistry C*, 2018, **122**, 6340.

94 D. Escudero, in *Transition Metals in Coordination Environments: Computational Chemistry and Catalysis Viewpoints*, eds. E. Broclawik, T. Borowski and M. Radoń, Springer International Publishing, Cham, 2019, p. 259.

95 I. Soriano-Díaz, E. Ortí and A. Giussani, *Dalton Transactions*, 2023, **52**, 10437.

96 D. Hernández-Castillo, R. E. P. Nau, M. A. Schmid, S. Tschierlei, S. Rau and L. González, *Angewandte Chemie International Edition*, 2023, **62**, e202308803.

97 P. Kumar, M. Pérez-Escribano, D. M. E. van Raamsdonk and D. Escudero, *Journal of Physical Chemistry A*, 2023, **127**, 7241.

98 N. Singh, G. H. Noh, H. Mubarok, C. W. Kim, M. H. Lee and J. Lee, *Polyhedron*, 2022, **227**, 116096.

99 J. Kang, R. Zaen, J. H. Lee, H. Hwang, K. M. Park, S. C. Kim, J. Y. Lee and Y. Kang, *Chemical Engineering Journal*, 2022, **431**, 134249.

100 B.-S. Yun, S.-Y. Kim, J.-H. Kim, S. Lee, H.-J. Son and S. O. Kang, *J Mater Chem C Mater*, 2022, **10**, 4196.

101 Y. Luo, Z. Chen, Z. Xu and D. Tang, *New Journal of Chemistry*, 2023, **47**, 3793.

102 J. Troya, M. M. Quesada-Moreno, J. R. Jiménez and J. M. Herrera, *New Journal of Chemistry*, 2023, **47**, 4577.

103 R. Gupta, P. Sahni, S. K. Jana, A. Negi and A. K. Pal, *Dalton Transactions*, 2023, **52**, 15597.

104 M. Santander-Nelli, B. Boza, F. Salas, D. Zambrano, L. Rosales and P. Dreyse, *Molecules*, 2022, **27**, 2623.

105 Y. Luo, L. Tang, Z. Chen, Z. Xu, J. Hu and D. Tang, *New Journal of Chemistry*, 2023, **47**, 8131.

106 T. J. Penfold, E. Gindensperger, C. Daniel and C. M. Marian, *Chem Rev*, 2018, **118**, 6975.

107 L. Tang, J. Gao, Y. Luo, Y. Cheng, L. Liu, D. Zheng, L. Liang, J. Hu and T. Luo, *New Journal of Chemistry*, 2023, **47**, 15076.

108 Z. Shuai, *Chin J Chem*, 2020, **38**, 1223.

109 S. Madronich, *Journal of Geophysical Research: Atmospheres*, 1987, **92**, 9740.

110 S. Madronich and S. Flocke, in *Environmental Photochemistry*, 1999, p. 1.

111 V. Vaida, *International Journal of Photoenergy*, 2005, **7**, 61.

112 J. C. Tully and R. K. Preston, *J Chem Phys*, 1971, **55**, 562–572.

113 R. Crespo-Otero and M. Barbatti, *Chem Rev*, 2018, **118**, 7026.

114 M. Barbatti, *Wiley Interdiscip Rev Comput Mol Sci*, 2011, **1**, 620.

115 E. Marsili, A. Prlj and B. F. E. Curchod, *Journal of Physical Chemistry A*, 2022, **126**, 5420.

116 J. Janoš, I. S. Vinklárek, J. Rakovský, D. P. Mukhopadhyay, B. F. E. Curchod, M. Fárník and P. Slavíček, *ACS Earth Space Chem*, 2023, **7**, 2275–2286.

117 L. Hutton and B. F. E. Curchod, *ChemPhotoChem*, 2022, **6**, e202200151.

118 A. Prlj, D. Hollas and B. F. E. Curchod, *Journal of Physical Chemistry A*, 2023, **127**, 7400.

119 E. Antwi, R. E. Bush, B. Marchetti and T. N. V Karsili, *Physical Chemistry Chemical Physics*, 2022, **24**, 16724.

120 J. Yang, Y. Li, L. Makroni and F. Liu, *Physical Chemistry Chemical Physics*, 2022, **24**, 22531.

121 E. Antwi, N. A. Packer, J. M. Ratliff, B. Marchetti and T. N. V Karsili, *Photochem Photobiol*, 2023, **99**, 1072.

122 C. A. Poirier, L. M. Guidry, J. M. Ratliff, V. J. Esposito, B. Marchetti and T. N. V Karsili, *Journal of Physical Chemistry A*, 2023, **127**, 6377.

123 G. Wang, T. Liu, M. Zou, T. N. V Karsili and M. I. Lester, *Physical Chemistry Chemical Physics*, 2023, **25**, 7453.

124 A. Saiz-Lopez, A. U. Acuña, A. S. Mahajan, J. Z. Dávalos, W. Feng, D. Roca-Sanjuán, J. Carmona-García, C. A. Cuevas, D. E. Kinnison, J. C. Gómez Martín, J. S. Francisco and J. M. C. Plane, *Geophys Res Lett*, 2022, **49**, e2022GL097953.

125 S. Mai, P. Marquetand and L. González, *Wiley Interdiscip Rev Comput Mol Sci*, 2018, **8**, e1370.

126 S. Pérez-Hoyos, A. Sánchez-Lavega, A. García-Muñoz, P. G. J. Irwin, J. Peralta, G. Holsclaw, W. M. McClintock and J. F. Sanz-Requena, *J Geophys Res Planets*, 2018, **123**, 145.

127 D. V Titov, N. I. Ignatiev, K. McGouldrick, V. Wilquet and C. F. Wilson, *Space Sci Rev*, 2018, **214**, 126.

128 J. B. Pollack, O. B. Toon, R. C. Whitten, R. Boese, B. Ragent, M. Tomasko, L. Esposito, L. Travis and D. Wiedman, *J Geophys Res Space Phys*, 1980, **85**, 8141.

129 B. N. Frandsen, P. O. Wennberg and H. G. Kjaergaard, *Geophys Res Lett*, 2016, **43**, 11146.

130 B. N. Frandsen, S. Farahani, E. Vogt, J. R. Lane and H. G. Kjaergaard, *Journal of Physical Chemistry A*, 2020, **124**, 7047.

131 B. N. Frandsen, P. O. Wennberg and H. G. Kjaergaard, *Geophysical Research Letters*, 2016, **43**, 11,146-11,155.

132 J. P. Pinto, J. Li, F. P. Mills, E. Marcq, D. Evdokimova, D. Belyaev and Y. L. Yung, *Nat Commun*, 2021, **12**, 175.

133 Z. Wu, H. Wan, J. Xu, B. Lu, Y. Lu, A. K. Eckhardt, P. R. Schreiner, C. Xie, H. Guo and X. Zeng, *Chemical Communications*, 2018, **54**, 4517.

134 A. Francés-Monerris, J. Carmona-García, T. Trabelsi, A. Saiz-Lopez, J. R. Lyons, J. S. Francisco and D. Roca-Sanjuán, *Nat Commun*, 2022, **13**, 4425.